https://doi.org/10.5194/acp-2019-764
Preprint. Discussion started: 30 September 2019

Atmospheric Chemistry and Physics Discussions

The conclusive impact of aerosols vertical structure on low-atmosphere stability and its critical role in aerosol-PBL interaction

Tianning Su[1], Zhanqing Li[1,2*], Chengcai Li[3], Jing Li[3], Wenchao Han[1,2], Chuanyang Shen[3,4], Wangshu Tan[3], Jianping Guo[5]

[1]Department of Atmospheric and Oceanic Sciences & ESSIC, University of Maryland, College Park, Maryland 20740, USA

[2]State Key Laboratory of Earth Surface Processes and Resource Ecology and College of Global Change and Earth System Science, Beijing Normal University, 100875, Beijing, China

[3]Department of Atmospheric and Oceanic Sciences, Peking University, Beijing 100871, China

[4]Department of Earth, Atmospheric and Planetary Sciences, Massachusetts Institute of Technology, Cambridge, MA, USA

[5]State Key Laboratory of Severe Weather, Chinese Academy of Meteorological Sciences, Beijing 100081, China

* Correspondence to: zli@atmos.umd.edu

https://doi.org/10.5194/acp-2019-764
Preprint. Discussion started: 30 September 2019

Atmospheric Chemistry and Physics Discussions
Open Access

Abstract. Aerosol-planetary boundary layer (PBL) interaction was proposed as an important mechanism to stabilize atmosphere and exacerbate surface air pollution. Despite the tremendous progress made in understanding this process, its magnitude and significance still bear large uncertainties and vary largely with aerosol distribution and meteorological conditions. In this study, we particularly focus on the role of aerosol vertical distribution on thermodynamic stability and PBL development by jointly using the micropulse lidar, sun-photometer, and radiosonde measurements over Beijing. Despite complex aerosol vertical distributions, the cloud-free aerosol structures can be classified into three types: well-mixed, decreasing with height, and the inversed. Under these different aerosol vertical structures, the aerosol-PBL relationships and the diurnal cycles of the PBLH and $PM_{2.5}$ show distinct characters. The vertical distribution of aerosol radiative forcing differs drastically with strong heating in the lower, mid, and upper PBL respectively. Such a discrepancy in heating rate affects the atmospheric buoyancy and stability differently in the three distinct aerosol structures. Absorbing aerosol have a weak effect of stabilizing the low-atmosphere under the decreasing structure than under the inverse structure. As a result, the aerosol-PBL interaction can be strengthened by the inverse aerosol structure and can be potentially neutralized by the decreasing structure. Moreover, aerosols can both enhance and suppress the PBL stability, leading to both positive and negative feedback loops. This study attempts to improve our understanding of aerosol-PBL interaction, which shows the importance of the observation constraint of aerosol vertical distribution for simulating the interaction and consequent feedbacks.

https://doi.org/10.5194/acp-2019-764
Preprint. Discussion started: 30 September 2019

1. Introduction

Aerosols critically impact on the Earth's climate through aerosol-cloud interactions (ACI) and aerosol-radiation interactions (ARI), and continue to contribute the considerable uncertainty to quantifications and interpretations of the Earth's changing radiation budget and hydrological cycles (Charlson et al., 1992; Ackerman et al., 2004; Boucher et al., 2013; Li et al., 2011, 2017a; Guo et al., 2017; 2018). Despite the great advances made in observation and modeling studies of the aerosol effects in the past decades, it is still a challenge to accurately quantify the effects on the climate system due to inadequate understanding of some mechanisms and strong variations in aerosol type, loading, and vertical distribution (Haywood and Boucher, 2000; Carslaw et al., 2013; Huang et al., 2015; Guo et al., 2016a; Li et al., 2016; Wang et al., 2019). Aerosols are known to interact with thermodynamic stability through ARI (Atwater, 1971; Bond et al., 2013). Absorbing aerosols can stabilize the atmosphere (Ramanathan et al., 2001; Wang et al., 2013; Ding et al., 2016), whereas they may also enhance convection and precipitation under certain conditions (Menon et al., 2002; Li et al., 2017).

Thermodynamic stability in the PBL dictates the PBL development (Garret 1994; Zhang et al., 2018), thereby dominating the vertical dissipation of surface pollutants to some degrees. Aerosols in turn have important feedbacks on the stability in PBL, depending on the aerosol properties, especially of the light absorption aerosols (e.g., black, organic, and brown carbon). However, due to large uncertainties in aerosol radiative forcing, it remains a challenge to quantify the impact of aerosols on thermodynamic stability and PBL development. Conventionally, increasing the aerosol

https://doi.org/10.5194/acp-2019-764
Preprint. Discussion started: 30 September 2019

Atmospheric Chemistry and Physics Discussions

absorption tends to stabilize the atmosphere, leading to reduced PBL height (PBLH). A more stable atmosphere and lower PBLH will in turn increase the surface aerosol loading, which is the well-established positive feedback loop in the aerosol-PBL interaction (e.g., Wang et al., 2015; Ding et al., 2016; Petäjä et al., 2016; Dong et al., 2017; Zou et al., 2017; Q. Huang et al., 2018; Z. Wang et al., 2018). However, such a positive feedback loop may not be real for all situations and is subject to confounding factors such as aerosol type, aerosol vertical distribution, soil moisture, and PBL regime (Guo et al., 2019; Lou et al., 2019). Geiß et al. (2017) reported the ambiguous relationships between surface aerosol loading and PBLH, while our previous study revealed weak correlations between surface pollutants and the PBLH in mountainous or clean regions (Su et al., 2018). A recent study by Lou et al. (2019) shows that aerosol has an even positive correlation with PBLH under the stable PBL, indicating the thermodynamic conditions in the PBL really matters.

Among others, numerical models are one of the viable methods to determine the aerosol impacts on stability and PBL (e.g. Ding et al., 2016; Y. Wang et al., 2018; Zhou et al., 2018; Wang et al., 2014). The aerosol optical depths (AOD), a measure of aerosol columnar loading, is usually taken into account in model simulations. However, aerosol vertical distribution in models is generally prescribed and may differ largely from the real situation, which highly varies in the PBL and is closely linked to the significant uncertainties in aerosol radiative effects. With observational constraints, the role of aerosol vertical distribution in aerosol-PBL interactions warrants a further investigation.

Coincidently, we have ample observational datasets over Beijing, including aerosol

https://doi.org/10.5194/acp-2019-764
Preprint. Discussion started: 30 September 2019

vertical distribution derived from lidar, optical properties derived from sun-photometer, the profiles of meteorological variables from radiosonde (RS), as well as surface $PM_{2.5}$ and meteorological parameters. Based on these measurements, a radiative transfer model is used to simulate the vertical profiles of aerosol radiative forcing that are employed to investigate the impact of aerosols on the buoyancy in the lower atmosphere.

The paper is structured as follows: Section 2 introduces the datasets and methods used. The analyses of aerosol-PBL interaction under different aerosol vertical structures are presented in Section 3. Section 5 discusses the results with a brief summary.

2. Data and Method

2.1. Site Description

In this study, we utilized data from multiple sources in Beijing, a megacity located at North China Plain. As one of the most densely populated and well-urbanized regions in the world, Beijing is a polluted region with high concentrations of absorbing aerosols (Zhang et al., 2019). The micropulse lidar (MPL) located at Beijing was operated continuously by Peking University (39.99°N, 116.31°E) from Mar 2016 to Dec 2018, with a temporal resolution of 15s and a vertical resolution of 15m. Due to incomplete laser pulses correction, the near-surface blind zones for lidar is ~0.15 km. Background subtraction, saturation, after-pulse, overlap, and range corrections are applied to raw MPL data to calculate the normalized signals (Yang et al., 2013; Su et al., 2018). The MPL data on raining days are excluded. Level 1.5 AOD and single-scattering albedos (SSA) are employed at multiple wavelengths (i.e. 0.44/0.5/0.67/0.87/1.02μm) from the

https://doi.org/10.5194/acp-2019-764
Preprint. Discussion started: 30 September 2019

Beijing RADI (40°N, 116.38°E) Aerosol Robotic Network (AERONET) site during 2011–2018, at cloud-free conditions (Holben et al., 1998; Zhang et al., 2017; Smirnov et al., 2000). The radiosonde (RS) station (39.80°N, 116.47°E) of Beijing is operated by China Meteorological Administration, which is ~25 km from the MPL site. The variables observed at the RS station include the meteorology data and profiles of water vapor, temperature, pressure and wind. The vertical resolution of RS is altitude dependent and generally less than 8 m (Guo et al., 2016b; Zhang et al., 2018). RS is routinely launched at 0800 Local Time (LT) and 2000 LT for each day, and also is launched at 1400 LT in summer (June-July-August). The RS measurements are collected during 2011–2018. To reduce small scale bias and obtain a stable regional variation of particulate matter with the diameter smaller than 2.5 μm ($PM_{2.5}$), we acquire mean $PM_{2.5}$ data from twenty environmental monitoring stations within 20 km from the lidar site, including one station of Beijing Embassy of United States. The topography of Beijing is presented in Figure 1. The green square indicates the MPL site, and the yellow triangle indicates the AERONET station. The brown star represents the radiosonde (RS) station, and the red pink dots represent the $PM_{2.5}$ sites.

2.2. Statistical Analysis Methods

Here the statistical significance is tested by two independent statistical methods, namely the least squares regression and the Kendall' tau test (Mann, 1945; Kendall, 1975). Least squares regression typically assumes a Gaussian data distribution in the trend analysis, whereas the MK test is a nonparametric test without any assumed functional form. The latter is more suitable for data that do not follow a certain

https://doi.org/10.5194/acp-2019-764
Preprint. Discussion started: 30 September 2019

Atmospheric Chemistry and Physics Discussions

distribution. To improve the robustness of the analysis, a relationship is considered to be significant when the confidence level is above 99% for both least squares regression and the MK test. Hereafter, "significant" indicates the correlation is statistically significant at the 99% confidence level.

In this study, we primarily use linear fit method to build the relationships between different parameters, and the Pearson correlation coefficient derived from linear regression analysis measures the degree to which the data fit a linear relationship. However, following our recent work (Su et al., 2018), the inverse fitting ($f(x) = {}^{A}/_{x} + B$) is used to establish the relationship between PBLH and $PM_{2.5}$. During this time, the magnitude of correlation coefficient is designed to measure the degree to which the data fit an inverse relationship. Since the relationship between the PBLH and $PM_{2.5}$ is non-linear, the inverse fitting is more suitable to characterize this relationship.

2.3. PBLH and buoyancy derived from RS

The vertical resolution varies according to the balloon ascending rate, and RS is recorded every 1.2s, which represents an approximate vertical resolution of 5–8 m. Prior to the retrieval of PBLH, we further resample the radiosonde data to achieve a vertical resolution of 5-hPa with linear interpolation. We follow a well-established method developed by Liu and Liang (2010) to derive the PBLH based on the profiles of potential temperature gradient that takes account of different stability conditions. In this study, we only focus on PBL driven by buoyancy, and thus, the PBL driven by the low-level jets will be excluded using the wind profiles from radiosonde (Liu and Liang, 2010; Miao et al., 2018).

https://doi.org/10.5194/acp-2019-764
Preprint. Discussion started: 30 September 2019

The static stability in atmosphere is determined by the buoyancy force which can be expressed as (Wallace and Hobbs, 2006):

$$B = \frac{d^2z}{dt^2} = \frac{T' - T}{T} g = -g\Delta z \frac{1}{\theta}\frac{d\theta}{dz} \qquad (1)$$

where z is the height of the air parcel and t indicates the time. T' represents the temperature of the parcel and T represents the temperature of the environment and θ is the virtual potential temperature of environment. For a certain layer, the atmosphere is identified as a convective condition when the buoyancy is above zero, but is identified as a stable condition when the buoyancy is below zero. If the buoyancy is near zero, the atmosphere is under a neutral condition. Based on the identification method for PBL types (Liu and Liang, 2010; Zhang et al., 2018), we present profiles of buoyancy forcing for a stable, neutral, and convective PBL (Figure 2a). Clearly, the strongest upward or downward forcing occurs near the surface. Figure 2b-c further show the height dependent correlation coefficients between buoyancy and PBLH/$PM_{2.5}$ with an interpolation window of 0.2km. Noted the PBLH and surface $PM_{2.5}$ are fixed for the entire column, and the buoyancy is height-dependent. Due to the insufficient development of PBL, we do not use RS data at 0800 LT here. To exclude the impact induced by the dragging effects of rainfall, we only use the cases without precipitation within the past 24 hours. Strong upward buoyancy can uplift PBLH and mitigate the surface pollutants, especially in the low atmosphere. Thus, we integrate the buoyancy forcing within the lowest 1km (red line in Figure 2b-c), which is defined as the low-atmosphere buoyancy (LAB). As shown in Figure 3a-b, the LAB shows strong negative correlations with $PM_{2.5}$ but positive correlations with PBLH. The LAB also has

https://doi.org/10.5194/acp-2019-764
Preprint. Discussion started: 30 September 2019

significant negative correlations with absorbing aerosol optical depth. It could be partly caused by the stabilizing effect of absorbing aerosol on the atmosphere, which is widely reported in many previous studies (Wang et al., 2015; Ding et al., 2016; Petäjä et al., 2016; Dong et al., 2017; Li et al., 2017; X. Huang et al., 2018).

2.4. PBLH and AEC derived from MPL

MPL data from Beijing were used to retrieve the PBLH during daytime (0800-1900 LT). Multiple methods have been developed for retrieving the PBLH from MPL measurements, such as signal threshold (Melfi et al., 1985), maximum of the signal variance (Hooper and Eloranta, 1986), minimum of the signal profile derivative (Flamant et al., 1997), and wavelet transform (Cohn and Angevine, 2000; Davis et al., 2000; Su et al., 2017). To derive the PBLH from MPL data, we adopted previous well-established approaches with several refinements, which has already been validated by long-term data over Southern Great Plains (ARM SGP) site (Sawyer and Li, 2013; Su et al., 2019).

Initially, we identify the local maximum positions (range: 0.25-4km) in the covariance transform function collocated with a signal gradient larger than a certain threshold. We further estimated the shot noise (σ) induced by background light and dark current for each profile, and then set the certain threshold as 3σ. The initial PBLH retrieval (0800LT) is constrained by the PBLH value derived from morning RS. Then, the following PBLHs would be retrieved using a stability dependent model based on continuity. The boundary layer clouds are identified to diagnose the PBLH for cloudy cases. Figure 3d presents the comparison of summertime PBLH results derived from

https://doi.org/10.5194/acp-2019-764
Preprint. Discussion started: 30 September 2019

MPL and RS at 1400 LT, and the agreement is reasonably good (R=0.77).

Multiple studies have provided a well-established algorithm to retrieve the vertical profiles of aerosol extinction coefficient (AEC) from MPL (eg., Fernald, 1984; Klett, 1985; Liu et al., 2012). Then, the Klett method is further applied for retrieving extinction profiles (Klett, 1985). The column-averaged extinction-to-backscatter ratio (so-called lidar ratio) is an important parameter in the retrieval processes and is constrained using AOD at 0.5μm derived from AERONET. The overall uncertainties from overlap function, lidar ratio, effects of multiple scattering, and noises are estimated to fall within a range of 20-30% in the retrieval processes (He et al., 2006).

2.5. Estimation of the impacts of aerosols on buoyancy

To illustrate the vertical profile of aerosol radiative forcing, the Santa Barbara DISORT Atmospheric Radiative Transfer (SBDART) model (Ricchiazzi et al., 1998) was used to simulate the atmospheric heating rate (dT/dt) induced by aerosol (Liu et al., 2012; Dong et al., 2017). The integrated aerosol inputs include AODs, and SSAs (i.e., 0.44, 0.67, 0.87 and 1.02μm) retrieved from AERONET measurements, as well as the AEC profiles at 0.5μm obtained from the MPL. We also use the MODIS surface reflectance as the additional inputs (https://modis.gsfc.nasa.gov/data/dataprod/mod09.php). We further use heating rate induced by aerosols to estimate the impacts of aerosols on buoyancy.

Theoretically, the rate of change in buoyancy for a certain layer can be expressed as:

https://doi.org/10.5194/acp-2019-764
Preprint. Discussion started: 30 September 2019

$$\frac{dB}{dt}=\frac{d}{dt}\left(\frac{T_0-\Gamma_d\Delta z-T}{T}g\right)=\frac{\left(\frac{dT_0}{dt}-\frac{dT}{dt}\right)T+\frac{dT}{dt}(\Gamma_d-\Gamma)\Delta z}{T^2}g \qquad (2)$$

where most parameters are defined in the same way as in Eq. (1), and Γ_d (Γ) represents the dry adiabatic lapse rate (environmental lapse rate). We will primarily focus on the change rate in buoyancy during noontime (1100-1500LT), when PBL is well developed and aerosol radiative forcing is strong. The change rate in buoyancy (dB/dt) induced by aerosols is largely determined by aerosol heating rate, which can be produced by the radiative transfer model. Additional inputs include environmental lapse rate and temperature, which are obtained from noontime RS in the summer. For other times, the environmental lapse rate and temperature are obtained from MERRA-2 reanalysis data, which assimilates coarse-resolution RS observation (Rienecker et al., 2011). In this way, we can estimate dB/dt induced by aerosols with a primary focus on daytime. Noted the errors in MERRA-2 data would lead to the uncertainties in the estimated dB/dt. 1~3 K uncertainties in MERRA-2 temperature (Gelaro et al., 2017) lead to 1-3% relative biases in the estimated dB/dt. Considering the large variation in dB/dt under different aerosol structures, the biases resulting from MERRA-2 data are not a very serious issue.

3. Results

3.1. Classification of different aerosol structure scenarios

By altering the adiabatic heating rate of the atmosphere, the aerosol vertical distribution is of great importance to the PBL. Based on cloud-free AEC profiles in the PBL, aerosol vertical structures can be classified into three types: well-mixed, decreasing with height, and inverse. If AEC varies by less than 20% within the lowest 80% of PBL, it is considered a well-mixed structure. For the other cases, a decreasing structure indicates a peak in AEC near the surface, and the inverse structure indicates a peak in AEC in the middle or upper PBL.

To investigate the vertical variation of AEC within the PBL, the evolution of PBLH has been taken into account. Following previous studies (Kuang et al., 2017; Ferrero et al., 2014), the vertical profiles were normalized by introducing a standardized height (H_s), which was calculated as follows:

$$H_s = \frac{z - PBLH}{PBLH} \qquad (3)$$

where z is the height above the ground and H_s is 0 at the PBL top and -1 at ground level. Then, the normalized vertical profiles of AEC during noontime are shown in Figure 4. Since a temperature inversion located at the PBL top traps moisture and aerosols, there is a sharp decrease in the AEC from the PBL upper boundary to free atmosphere. The aerosol vertical distribution largely varies depending on different conditions, but share similar features under different aerosol structure patterns. Despite complex aerosol vertical distributions, these three types of profiles can account for more than 85% of cloud-free cases.

3.2. PBLH and $PM_{2.5}$ under different aerosol structure scenarios

Absorbing aerosols trend to have positive feedback with PBLH, while aerosols vertical distribution plays a critical role in this process. We investigate the relationship between MPL-derived PBLH and $PM_{2.5}$ for absorbing (SSA $\leq$ 0.85) or weakly absorbing (SSA > 0.9) aerosols under inverse/declining aerosol structures (Figure 5).

https://doi.org/10.5194/acp-2019-764
Preprint. Discussion started: 30 September 2019

In general, there are stronger correlations between PBLH and $PM_{2.5}$ under inverse aerosols structure. Under such structure, the PBLH-$PM_{2.5}$ correlation also remains considerably stronger for absorbing than weakly absorbing cases. This is likely caused by substantial heating in the upper PBL, which would facilitate the formation of temperature inversion and further increase the stability in the PBL. While, under declining aerosols structure, the aerosols may not significantly redistribute the adiabatic energy. This phenomenon indicates that the absorbing aerosol could play a more important role in the inverse aerosol structure.

The diurnal cycles of AEC, PBLH, and $PM_{2.5}$ for different aerosol vertical structures are presented in Figure 6 based on the measurements made in Beijing. High humidity cases (RH > 80%) and strong wind cases (wind speed > 5m s^{-1}) are excluded. Theoretically, $PM_{2.5}$ should generally decrease with increasing PBLH in the morning and forenoon due to the dilution effect. This situation is demonstrated clearly for decreasing structures. However, $PM_{2.5}$ continuously grows during the daytime under inverse aerosol structures, regardless of the PBLH diurnal cycle. Despite the diurnal variations of aerosol and PBL are controlled by many factors, the strong aerosol-stability interaction may be an underlying scheme that further enhances the surface aerosol loading during the daytime.

3.3. Aerosol radiative forcing under different aerosol structures

Figure 7 shows heating rates induced by aerosols for decreasing, well-mixed and inverse cases. The vertical distributions of the heating rate differ drastically with significant heating in the different parts of PBL. This is caused by substantial heating

https://doi.org/10.5194/acp-2019-764
Preprint. Discussion started: 30 September 2019

in the upper PBL, which would facilitate the formation of temperature inversion and further increase the stability in the PBL. Nonetheless, under the declining aerosol structure, the abundant aerosols in the bottom of PBL can cause a heating effect in the lower PBL, and hence, can potentially enhance the convection in PBL.

There are considerable differences in heating rate among the three distinct aerosol structures (Figure 8), which affects the atmospheric buoyancy and stability differently. On average, aerosols generally suppress buoyancy in the low atmosphere. Such an effect is quite notable for inverse structure and is insignificant for decreasing structure with large standard deviations. Absorbing aerosol is not very helpful for stabilizing low-atmosphere under the decreasing structure, but plays an important role under the inverse structure. As such, we expected the strongest aerosol-PBL interactions for absorbing cases under the inverse structure, which is consistent with the results in Figure 4. It should be noted that there are large variations in the impact of aerosol on buoyancy. Under an inverse structure, aerosol overwhelmingly enhance the stability in low-atmosphere, whereas, under decreasing structure, aerosols have the potential to either enhance or suppress the low-atmosphere stability depending on different cases.

Figure 9 illustrates the schematic diagram of the interactions between aerosols, stability, and the PBL. Overall, aerosol vertical structure critically affects the aerosol-PBL interaction. The inverse aerosol structure facilitates the formation of temperature inversion and further increases the stability and aerosol loading in the near surface. Therefore, the inverse aerosol structure may strengthen the aerosol-PBL interaction. Meanwhile, the aerosol-PBL interaction can be potentially neutralized by the decreasing structure. Moreover, aerosols can both enhance and suppress the PBL stability depending on different conditions, and lead to both positive and negative feedback loops (Figure 9). The positive feedback loop leads to strong aerosol-PBL interactions, while the negative feedback loop partly offset PBL's impacts on aerosol loading. It explains the paradox of the impact of the PBL on surface pollutants, since its magnitude, significance, and even sign reportedly varies or even reverses (Quan et al., 2013; Tang et al., 2015; Geiß et al., 2017; Su et al., 2018).

4. Summary and Discussions

Based on integrated aerosol and meteorological measurements over Beijing, the aerosol-PBL interaction is assessed under different aerosol vertical structures, which are decreasing, well-mixed, and inversely increasing with height, respectively. The aerosol-PBL relationships and the diurnal cycles of PBLH and $PM_{2.5}$ show distinct characteristics among the different aerosol vertical patterns. For the decreasing aerosol structure, $PM_{2.5}$ decreases in the morning and forenoon with relatively large PBLH growth rates. In this situation, absorbing aerosol is not very helpful in stabilizing low-atmosphere. Under the inverse aerosol structure, $PM_{2.5}$ continuously grows during daytime with relative low PBLH growth rate. This phenomenon could be a sign of the strong aerosol-PBL interaction. The aerosol radiative forcing in vertical scale for decreasing, well-mixed, and inverse aerosol structures differ drastically with strong heating in the lower, mid, and upper PBL respectively. Such a difference in heating rate affects the atmospheric buoyancy and stability differently in the three distinct aerosol structures.

Numerous studies used various models to simulate the aerosol-PBL interactions and consequent feedbacks (e.g. Ding et al., 2016; Z. Wang et al., 2018; Zhou et al., 2018; Wang et al., 2014). Aerosol vertical distribution highly varies in both temporal and vertical scales, and critically affect the aerosol radiative forcing. Nonetheless, the aerosol vertical distribution usually poorly represented in numerical models, due to a lack of observational constraints. This study reveals the important role of aerosol vertical distribution in aerosol-PBL interactions, which should be carefully taken into account in both observational analysis and model simulations.

In this study, we use column-averaged aerosol properties from AERONET. However, the vertical variations of single scattering albedo and aerosol type remains unknown, which can induce uncertainties in the estimation of aerosol effects. In the future, we plan to use aircraft data from field campaigns to better account for its influences for different types of aerosols of different properties.

Data availability. The hourly $PM_{2.5}$ data are released by the Ministry of Environmental Protection of China (data link: http://113.108.142.147:20035/emcpublish). The MERRA-2 reanalysis data are publicly available at https://disc.gsfc.nasa.gov/datasets?keywords=merra%202&page=1. The AERONET data are publicly available at https://aeronet.gsfc.nasa.gov. The meteorological data are provided by the data center of China Meteorological Administration (data link: http://data.cma.cn/en).

Author contribution. T.S. and Z.L. conceptualized this study. T.S. carried out the analysis, with comments from other co-authors. C.L., J.L. and W.T. carried out the MPL observation. J.G. provided auxiliary data. W.H., C.S., W.T., and J.G. provided useful suggestions for the discussion. T.S. and Z.L. interpreted the data and wrote the manuscript with contributions from all co-authors.

Competing interests. The authors declare that they have no conflict of interest.

Acknowledgements. This work is supported in part by grants from the National Science Foundation (AGS1837811 and AGS1534670). The authors would like to acknowledge Prof. Zhengqiang Li for his effort in establishing and maintaining the Beijing RADI AERONET site. We thank the provision of $PM_{2.5}$ by the Ministry of Environmental Protection of the People's Republic of China, and also thank the provision of meteorological data and radiosonde by China Meteorological Administration. We extend sincerest thanks to the MERRA teams for their datasets.

References

Ackerman, A. S., Kirkpatrick, M. P., Stevens, D. E., and Toon, O. B., 2004. The impact of humidity above stratiform clouds on indirect aerosol climate forcing. Nature, 432, 1014–1017. https://doi.org/10.1038/nature03174.

Atwater, M. A., 1971. The radiation budget for polluted layers of the urban environment. Journal of Applied Meteorology, 10(2), 205–214.

Bond, T. C., Doherty, S. J., Fahey, D. W., Forster, P. M., Berntsen, T., DeAngelo, B. J., Flanner, M. G., Ghan, S., Kärcher, B., Koch, D. and Kinne, S., 2013. Bounding

https://doi.org/10.5194/acp-2019-764
Preprint. Discussion started: 30 September 2019

the role of black carbon in the climate system: A scientific assessment. Journal of Geophysical Research: Atmospheres, 118(11), 5380–5552.

Boucher, O., Randall, D., Artaxo, P., Bretherton, C., Feingold, G., Forster, P., Kerminen, V. M., Kondo, Y., Liao, H., Lohmann, U., and Rasch, P., 2013. Clouds and aerosols, in: Climate Change 2013: The Physical Science Basis. Contribution of Working Group I to the Fifth Assessment Report of the Intergovernmental Panel on Climate Change, 571–657, Cambridge Univ. Press, Cambridge, UK and New York, NY, USA.

Carslaw, K.S., Lee, L.A., Reddington, C.L., Pringle, K.J., Rap, A., Forster, P.M., Mann, G.W., Spracklen, D.V., Woodhouse, M.T., Regayre, L.A. and Pierce, J.R., 2013. Large contribution of natural aerosols to uncertainty in indirect forcing. Nature, 503(7474), p.67.

Charlson, R.J., Schwartz, S.E., Hales, J.M., Cess, R.D., Coakley, J.J., Hansen, J.E. and Hofmann, D.J., 1992. Climate forcing by anthropogenic aerosols. Science, 255(5043), pp.423-430.

Cohn, S. A. and Angevine, W. M.: Boundary layer height and entrainment zone thickness measured by lidars and wind-profiling radars, J. Appl. Meteorol., 39, 1233–1247, https://doi.org/10.1175/1520-0450(2000)039<1233:BLHAEZ>2.0.CO;2, 2000.

Davis, K. J., Gamage, N., Hagelberg, C. R., Kiemle, C., Lenschow, D. H., and Sullivan P. P.: An objective method for deriving atmospheric structure from airborne lidar observations. J. Atmos. Ocean. Tech., 17, 1455–1468, https://doi.org/10.1175/1520- 0426(2000)017<1455:AOMFDA>2.0.CO;2, 2000

Ding, A.J., Huang, X., Nie, W., Sun, J.N., Kerminen, V.M., Petäjä, T., Su, H., Cheng, Y.F., Yang, X.Q., Wang, M.H. and Chi, X.G., 2016. Enhanced haze pollution by black carbon in megacities in China. Geophysical Research Letters, 43(6), pp.2873-2879.

Fernald, F.G., 1984. Analysis of atmospheric lidar observations: some comments. Applied optics, 23(5), pp.652-653.

Ferrero, L., Castelli, M., Ferrini, B.S., Moscatelli, M., Perrone, M.G., Sangiorgi, G., D'Angelo, L., Rovelli, G., Moroni, B., Scardazza, F. and Močnik, G., 2014. Impact of black carbon aerosol over Italian basin valleys: high-resolution measurements along vertical profiles, radiative forcing and heating rate. Atmospheric Chemistry and Physics, 14(18), pp.9641-9664.

Flamant, C., Pelon, J., Flamant, P.H. and Durand, P., 1997. Lidar determination of the entrainment zone thickness at the top of the unstable marine atmospheric boundary layer. Boundary-Layer Meteorology, 83(2), pp.247-284.

Geiß, A., Wiegner, M., Bonn, B., Schäfer, K., Forkel, R., Schneidemesser, E.V., Münkel, C., Chan, K.L. and Nothard, R., 2017. Mixing layer height as an indicator for urban air quality?. Atmospheric Measurement Techniques, 10(8), pp.2969-2988.

Gelaro, R., McCarty, W., Suárez, M.J., Todling, R., Molod, A., Takacs, L., Randles, C.A., Darmenov, A., Bosilovich, M.G., Reichle, R. and Wargan, K., 2017. The modern-era retrospective analysis for research and applications, version 2 (MERRA-2). Journal of Climate, 30(14), pp.5419-5454.

Guo, J., H. Liu, F. Wang, J. Huang, F. Xia, M. Lou, Y. Wu, J. Jiang, T. Xie, Y. Zhaxi, and Y. Yung, 2016. Three-dimensional structure of aerosol in China: A perspective from multi-satellite observations, Atmospheric Research, 178–179: pp.580–589.

Guo, J., Liu, H., Li, Z., Rosenfeld, D., Jiang, M., Xu, W., Jiang, J. H., He, J., Chen, D., Min, M., and Zhai, P., 2018. Aerosol-induced changes in the vertical structure of precipitation: a perspective of TRMM precipitation radar. Atmospheric Chemistry and Physics, 18, pp.13329–13343.

Guo, J., Miao, Y., Zhang, Y., Liu, H., Li, Z., Zhang, W., He, J., Lou, M., Yan, Y., Bian, L., and Zhai, P., 2016. The climatology of planetary boundary layer height in China derived from radiosonde and reanalysis data. Atmospheric Chemistry and Physics, 16, pp.13309–13319.

Guo, J., Su, T., Li, Z., Miao, Y., Li, J., Liu, H., Xu, H., Cribb, M. and Zhai, P., 2017. Declining frequency of summertime local-scale precipitation over eastern China from 1970 to 2010 and its potential link to aerosols. Geophysical Research Letters, 44(11), pp.5700-5708.

Guo, J., Y. Li, J. Cohen, J. Li, D. Chen, H. Xu, L. Liu, J. Yin, K. Hu, P. Zhai, 2019. Shift in the temporal trend of boundary layer height trend in China using long-term (1979–2016) radiosonde data. Geophysical Research Letters, 46 (11), pp.6080-6089

Guo, S., Hu, M., Zamora, M.L., Peng, J., Shang, D., Zheng, J., Du, Z., Wu, Z., Shao, M., Zeng, L. and Molina, M.J., 2014. Elucidating severe urban haze formation in China. Proceedings of the National Academy of Sciences, 111(49), pp.17373-17378.

Haywood, J. and Boucher, O., 2000. Estimates of the direct and indirect radiative forcing due to tropospheric aerosols: A review. Reviews of geophysics, 38(4), pp.513-543.

He, Q.S., Li, C.C., Mao, J.T., Lau, A.K.H. and Li, P.R., 2006. A study on the aerosol extinction-to-backscatter ratio with combination of micro-pulse LIDAR and MODIS over Hong Kong. Atmospheric Chemistry and Physics, 6(11), pp.3243-3256.

Holben, B.N., Eck, T.F., Slutsker, I., Tanre, D., Buis, J.P., Setzer, A., Vermote, E., Reagan, J.A., Kaufman, Y.J., Nakajima, T. and Lavenu, F., 1998. AERONET—A federated instrument network and data archive for aerosol characterization. Remote sensing of environment, 66(1), pp.1-16.

Huang, J., J. Guo, F. Wang, Z. Liu, M. -J. Jeong, H. Yu and Z. Zhang, 2015. CALIPSO inferred most probable heights of global dust and smoke layers, Journal of Geophysical Research-Atmospheres, 120(10), pp5085–5100,

Huang, Q., Cai, X., Wang, J., Song, Y. and Zhu, T., 2018. Climatological study of the Boundary-layer air Stagnation Index for China and its relationship with air pollution. Atmospheric Chemistry and Physics, 18(10), p.7573.

Huang, X., Wang, Z. and Ding, A., 2018. Impact of Aerosol-PBL Interaction on Haze Pollution: Multiyear Observational Evidences in North China. Geophysical Research Letters, 45(16), pp.8596-8603.

Klett, J.D., 1985. Lidar inversion with variable backscatter/extinction ratios. Applied

https://doi.org/10.5194/acp-2019-764
Preprint. Discussion started: 30 September 2019

Atmospheric Chemistry and Physics Discussions

optics, 24(11), pp.1638-1643.

Kuang, Y., Zhao, C.S., Tao, J.C., Bian, Y.X. and Ma, N., 2016. Impact of aerosol hygroscopic growth on the direct aerosol radiative effect in summer on North China Plain. Atmospheric Environment, 147, pp.224-233.

Li Z. et al. 2007: Preface to special section on East Asian Study of Tropospheric Aerosols: an International Regional Experiment (EAST-AIRE), J. Geophys. Res., D22S00, doi:10.1029/2007JD008853.

Li, Z., J. Guo, A. Ding, H. Liao, J. Liu, Y. Sun, T. Wang, H. Xue, H. Zhang, B. Zhu, 2017b. Aerosol and boundary-layer interactions and impact on air quality. National Science Review, nwx117. https://doi.org/10.1093/nsr/nwx117.

Li, Z., Niu, F., Fan, J., Liu, Y., Rosenfeld, D. and Ding, Y., 2011. Long-term impacts of aerosols on the vertical development of clouds and precipitation. Nature Geoscience, 4(12), p.888.

Li, Z., Rosenfeld, D., and Fan, J., 2017a. Aerosols and their Impact on Radiation, Clouds, Precipitation and Severe Weather Events, Oxford Encyclopedia in Environmental Sciences, 10.1093/acrefore/9780199389414.013.126.

Li, Z., W.K.-M. Lau, V. Ramanathan, et al., 2016. Aerosol and monsoon climate interactions over Asia. Rev. of Geophys., 54, 866–929. https://doi.org/10.1002/2015RG000500.

Liu, J., Zheng, Y., Li, Z., Flynn, C. and Cribb, M., 2012. Seasonal variations of aerosol optical properties, vertical distribution and associated radiative effects in the Yangtze Delta region of China. Journal of Geophysical Research: Atmospheres, 117(D16).

Lou, M., J. Guo, L. Wang, H. Xu, D. Chen, Y. Miao, Y. Lv, Y. Li, X. Guo, S. Ma, and J. Li, 2019. On the relationship between aerosol and boundary layer height in summer in China under different thermodynamic conditions. Earth and Space Science, 6(5), pp.887-901.

Melfi, S.H., Spinhirne, J.D., Chou, S.H. and Palm, S.P., 1985. Lidar observations of vertically organized convection in the planetary boundary layer over the ocean. Journal of climate and applied meteorology, 24(8), pp.806-821.

Menon, S., Hansen, J., Nazarenko, L. and Luo, Y., 2002. Climate effects of black carbon aerosols in China and India. Science, 297(5590), pp.2250-2253.

Miao, Y., Guo, J., Liu, S., Wei, W., Zhang, G., Lin, Y. and Zhai, P., 2018. The climatology of low‐level jet in Beijing and Guangzhou, China. Journal of Geophysical Research: Atmospheres, 123(5), pp.2816-2830.

Petäjä, T., Järvi, L., Kerminen, V.M., Ding, A.J., Sun, J.N., Nie, W., Kujansuu, J., Virkkula, A., Yang, X., Fu, C.B., Zilitinkevich, S., and M. Kulmala., 2016. Enhanced air pollution via aerosol-boundary layer feedback in China. Scientific Reports, 6. https://doi.org/10.1038/srep18998.

Quan, J., Gao, Y., Zhang, Q., Tie, X., Cao, J., Han, S., Meng, J., Chen, P. and Zhao, D., 2013. Evolution of planetary boundary layer under different weather conditions, and its impact on aerosol concentrations. Particuology, 11(1), pp.34-40.

Ramanathan, V.C.P.J., Crutzen, P.J., Kiehl, J.T. and Rosenfeld, D., 2001. Aerosols, climate, and the hydrological cycle. Science, 294(5549), pp.2119-2124.

https://doi.org/10.5194/acp-2019-764
Preprint. Discussion started: 30 September 2019

Atmospheric Chemistry and Physics
Discussions

Ricchiazzi, P., Yang, S., Gautier, C., and Sowle, D., 1998. SBDART: A research and teaching software tool for planeparallel radiative transfer in the Earth's atmosphere, B. Am. Meteorol. Soc., 79, 2101–2114, https://doi.org/10.1175/1520-0477(1998)079<2101:SARATS>2.0.CO;2.

Rienecker, M.M., Suarez, M.J., Gelaro, R., Todling, R., Bacmeister, J., Liu, E., Bosilovich, M.G., Schubert, S.D., Takacs, L., Kim, G.K. and Bloom, S., 2011. MERRA: NASA's modern-era retrospective analysis for research and applications. Journal of climate, 24(14), pp.3624-3648.

Sawyer, V., and Li, Z., 2013. Detection, variations and intercomparison of the planetary boundary layer depth from radiosonde, lidar, and infrared spectrometer, Atmos. Environ., 79, 518-528.

Smirnov, A., Holben, B.N., Eck, T.F., Dubovik, O. and Slutsker, I., 2000. Cloud-screening and quality control algorithms for the AERONET database. Remote sensing of environment, 73(3), pp.337-349.

Su, T., Li, J., Li, C., Xiang, P., Lau, A.K.H., Guo, J., Yang, D. and Miao, Y., 2017. An intercomparison of long-term planetary boundary layer heights retrieved from CALIPSO, ground-based lidar, and radiosonde measurements over Hong Kong. J. Geophys. Res. Atmos., 122(7), 3929- 3943.

Su, T., Li, Z. and Kahn, R., 2018. Relationships between the planetary boundary layer height and surface pollutants derived from lidar observations over China: regional pattern and influencing factors. Atmospheric Chemistry and Physics, 18(21), pp.15921-15935.

Su, T., Li, Z., and Kahn, R., 2019. A new method to retrieve the diurnal variability of planetary boundary layer height from lidar under different thermodynamic stability conditions. *Remote Sensing of Environment*., in review.

Tang, G., Zhang, J., Zhu, X., Song, T., Münkel, C., Hu, B., Schäfer, K., Liu, Z., Zhang, J., Wang, L. and Xin, J., 2016. Mixing layer height and its implications for air pollution over Beijing, China. Atmospheric Chemistry and Physics, 16(4), pp.2459-2475.

Wallace, J.M. and Hobbs, P.V., 2006. Atmospheric science: an introductory survey (Vol. 92). Elsevier.

Wang, H., Shi, G.Y., Zhang, X.Y., Gong, S.L., Tan, S.C., Chen, B., Che, H.Z. and Li, T., 2015. Mesoscale modelling study of the interactions between aerosols and PBL meteorology during a haze episode in China Jing–Jin–Ji and its near surrounding region–Part 2: Aerosols' radiative feedback effects. Atmospheric Chemistry and Physics, 15(6), pp.3277-3287.

Wang, J., Wang, S., Jiang, J., Ding, A., Zheng, M., Zhao, B., Wong, D.C., Zhou, W., Zheng, G., Wang, L. and Pleim, J.E., 2014. Impact of aerosol–meteorology interactions on fine particle pollution during China's severe haze episode in January 2013. Environmental Research Letters, 9(9), p.094002.

Wang, Y., A. Khalizov, M. Levy, R. Zhang, 2013. New directions: Light absorbing aerosols and their atmospheric impacts, Atmos. Environ., 81, pp.713-715.

Wang, Y., Li, Z., Zhang, Y., Du, W., Zhang, F., Tan, H., Xu, H., Fan, T., Jin, X., Fan, X. and Dong, Z., 2018. Characterization of aerosol hygroscopicity, mixing state, and

https://doi.org/10.5194/acp-2019-764
Preprint. Discussion started: 30 September 2019

CCN activity at a suburban site in the central North China Plain. Atmospheric Chemistry and Physics, 18(16), pp.11739-11752.

Wang, Z., Huang, X. and Ding, A., 2018. Dome effect of black carbon and its key influencing factors: a one-dimensional modelling study. Atmospheric Chemistry and Physics, 18(4), pp.2821-2834.

Wang, Z., Huang, X. and Ding, A., 2019. Optimization of vertical grid setting for air quality modelling in China considering the effect of aerosol-boundary layer interaction. Atmospheric Environment, 210, pp.1-13.

Yang, D., Li, C., Lau, A.K.H. and Li, Y., 2013. Long-term measurement of daytime atmospheric mixing layer height over Hong Kong. Journal of Geophysical Research: Atmospheres, 118(5), pp.2422-2433.

Zhang, W., J. Guo, Y. Miao, H. Liu, Y. Song, Z. Fang, J. He, M. Lou, Y. Yan, Y. Li, and P. Zhai, 2018. On the summertime planetary boundary layer with different thermodynamic stability in China: A radiosonde perspective. Journal of Climate, 31(4), pp. 1451 – 1465.

Zhang, Y., Li, Z., Zhang, Y., Li, D., Qie, L., Che, H. and Xu, H., 2017. Estimation of aerosol complex refractive indices for both fine and coarse modes simultaneously based on AERONET remote sensing products. Atmospheric Measurement Techniques, 10(9), pp.3203-3213.

Zhang, Y., Y. Li, J. Guo, Y. Wang, D. Chen, and H. Chen, 2019. The climatology and trend of black carbon in China from 12-year ground observations. Climate Dynamics, doi:10.1007/s00382-019-04903-0.

Zhou, M., Zhang, L., Chen, D., Gu, Y., Fu, T.M., Gao, M., Zhao, Y., Lu, X. and Zhao, B., 2018. The impact of aerosol-radiation interactions on the effectiveness of emission control measures. Environmental Research Letters.

Zou, J., Sun, J., Ding, A., Wang, M., Guo, W. and Fu, C., 2017. Observation-based estimation of aerosol-induced reduction of planetary boundary layer height. Advances in Atmospheric Sciences, 34(9), pp.1057-1068.

https://doi.org/10.5194/acp-2019-764
Preprint. Discussion started: 30 September 2019

Atmospheric Chemistry and Physics Discussions
Open Access
EGU

583 **Figures**

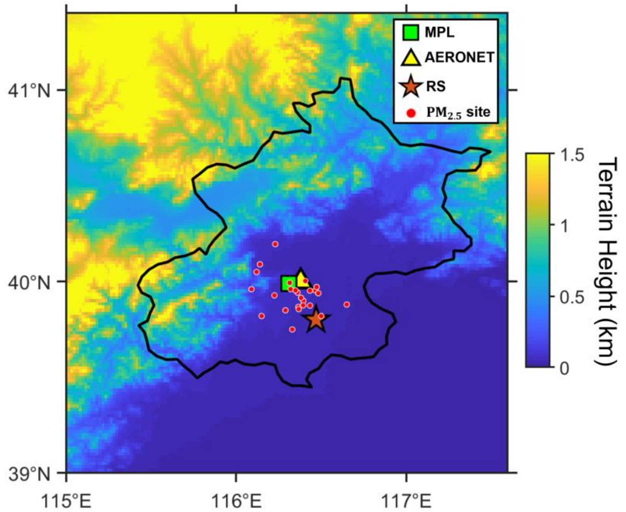

584

585 **Figure 1.** Topography condition of Beijing. The green square indicates the MPL site,
586 and the yellow triangle indicates the AERONET station. The brown star represents
587 radiosonde (RS) station, and the red pink dots represent the $PM_{2.5}$ sites.

588

589

590

591

592

593

594

https://doi.org/10.5194/acp-2019-764
Preprint. Discussion started: 30 September 2019

Atmospheric Chemistry and Physics Discussions

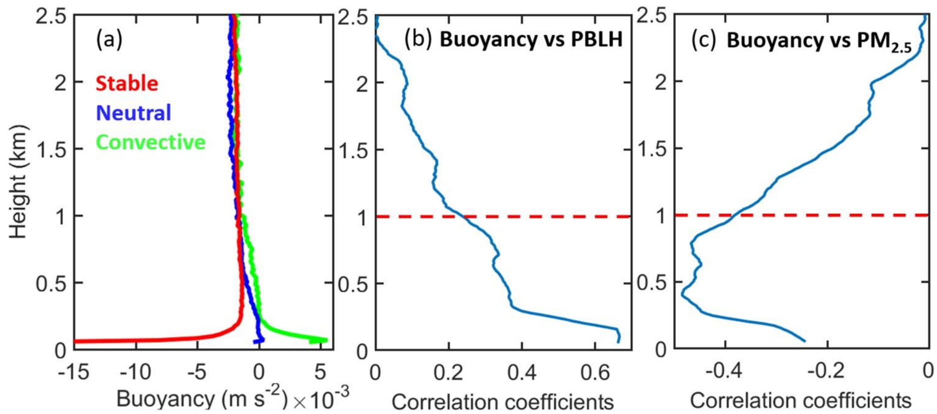

Figure 2. (a) Vertical profiles of buoyancy forcing under stable, neutral, and convective PBL. (b) Height-dependent correlation coefficients between buoyancy and PBLH. (c) Height-dependent correlation coefficients between buoyancy and surface $PM_{2.5}$. Noted the PBLH and surface $PM_{2.5}$ are fixed for the entire column, and the buoyancy is height-dependent. The buoyancy within low-atmosphere (1 km) exerts the most important impact on PBLH and surface $PM_{2.5}$. The buoyancy and PBLH are derived from RS at 1400 LT and 2000 LT

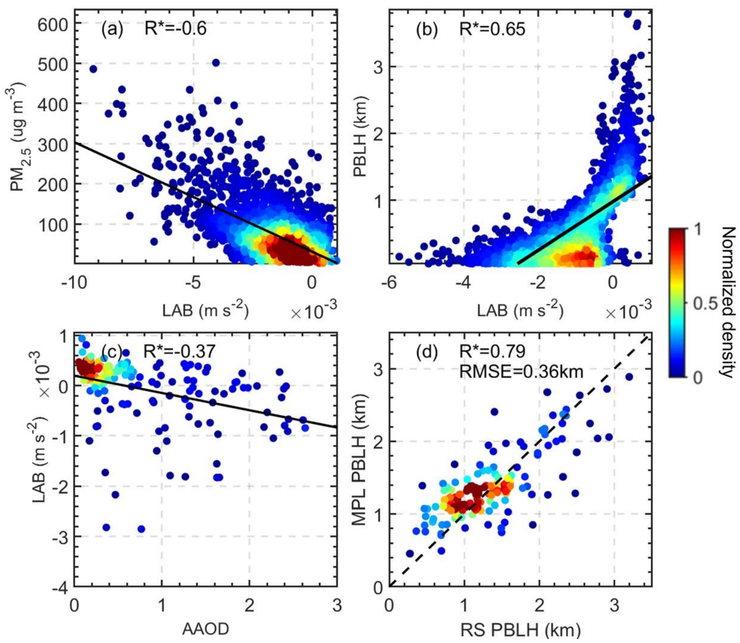

Figure 3. (a) The relationships between low-atmosphere buoyancy (LAB) and $PM_{2.5}$. (b) The relationships between LAB and PBLH. (c) The relationships between absorbing aerosol optical depth (AAOD) and LAB. In (a, b, c), the LAB and PBLH are derived from RS at 1400 LT and 2000 LT, and black solid lines indicate the linear regressions. (d) Comparison of PBLHs derived from MPL and RS at 1400 LT. Here and in the following analysis, R with asterisks indicates that the correlation is statistically significant at the 99% confidence level. The color-shaded dots indicate the normalized sample density.

https://doi.org/10.5194/acp-2019-764
Preprint. Discussion started: 30 September 2019

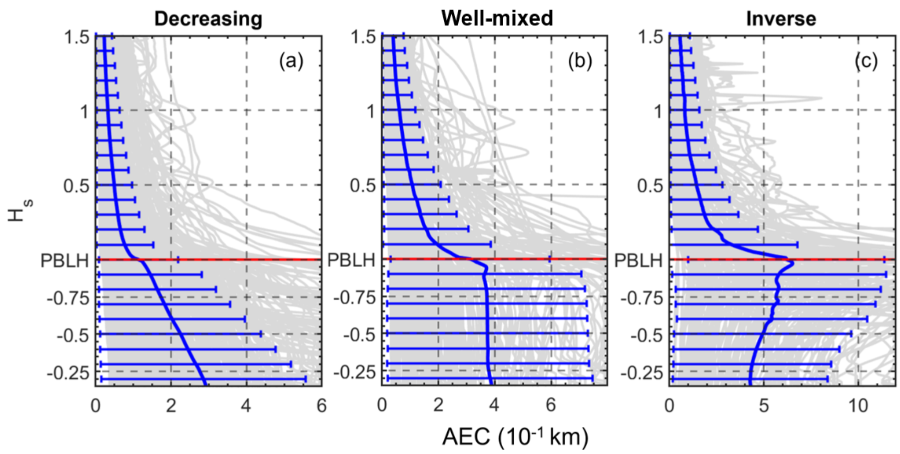

Figure 4. The normalized vertical profiles of aerosol extinction coefficients (AEC) under (a) decreasing, (b) well-mixed, and (c) inverse structures. The red line marks the position of the PBLH, the solid blue lines represent the average profile of corresponding profiles, and the error-bars represent the standard deviations.

https://doi.org/10.5194/acp-2019-764
Preprint. Discussion started: 30 September 2019

Atmospheric Chemistry and Physics
Discussions

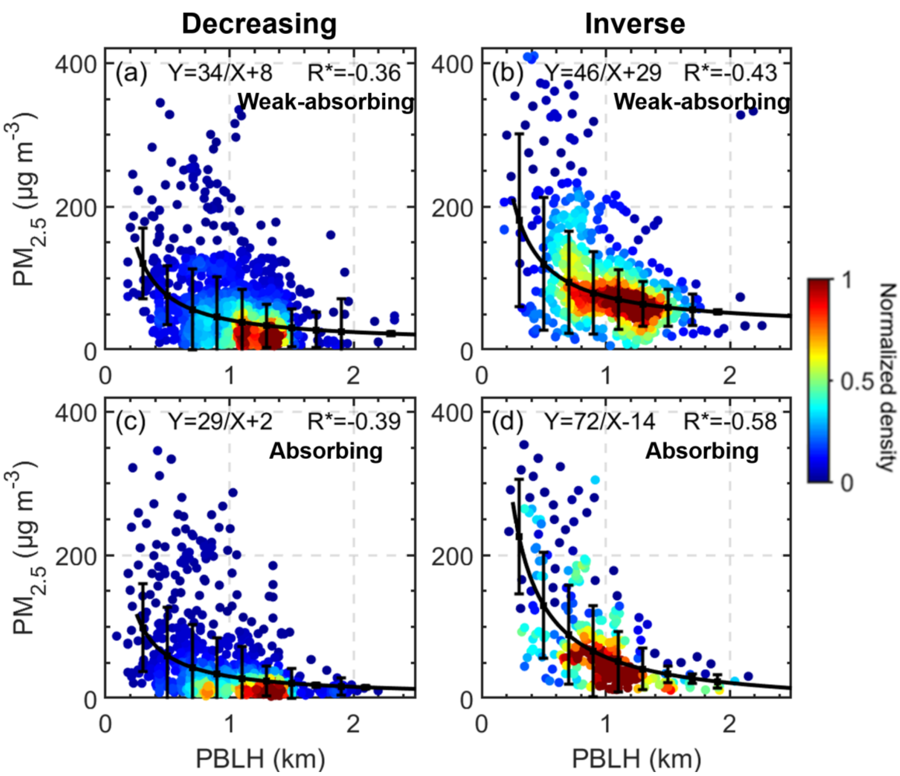

Figure 5. The relationship between MPL-derived PBLH and $PM_{2.5}$ for (a) weak-absorbing and (c) absorbing under decreasing aerosols structure. The relationship between MPL-derived PBLH and $PM_{2.5}$ for (b) weak-absorbing and (d) absorbing under inverse aerosols structure. The black lines represent the inverse fit, and the whiskers indicate the standard deviations. The detailed fitting functions are given at the top of each panel, along with the correlation coefficient for the inverse fit.

https://doi.org/10.5194/acp-2019-764
Preprint. Discussion started: 30 September 2019

Atmospheric Chemistry and Physics Discussions

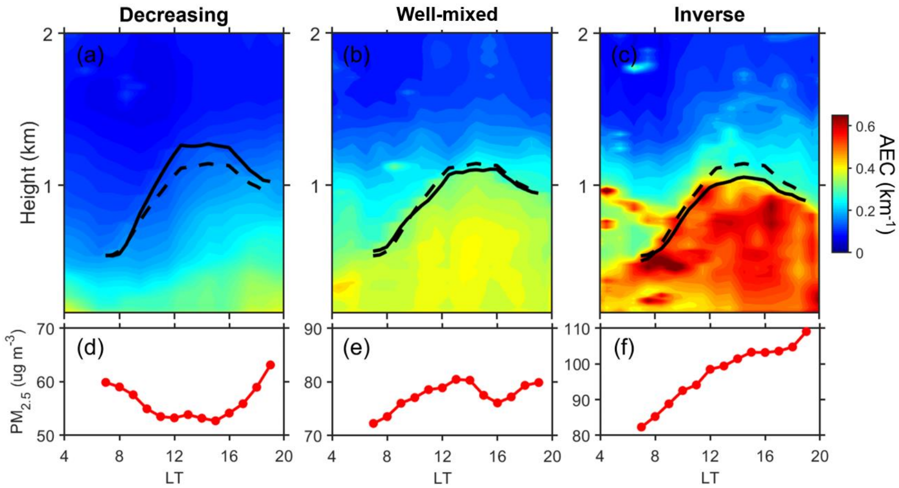

Figure 6. Diurnal variations in AEC for (a) decreasing, (b) well-mixed, and (c) inverse structures. The solid black lines indicate the corresponding PBLH diurnal cycles. The dashed black line represents the mean PBLH diurnal cycle. (d, e, f) The corresponding diurnal variations in $PM_{2.5}$.

https://doi.org/10.5194/acp-2019-764
Preprint. Discussion started: 30 September 2019

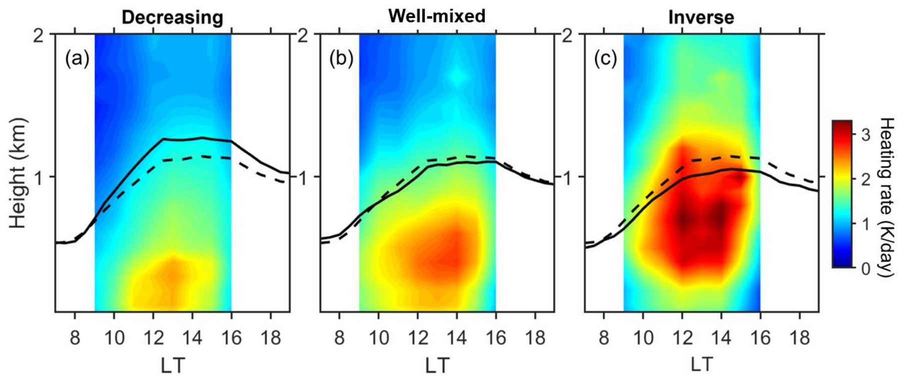

Figure 7. The profiles of aerosol radiative forcing for (a) decreasing, (b) well-mixed, and (c) inverse structures of aerosol loading. The solid black lines indicate the corresponding PBLH diurnal cycles. The dashed black line represents the mean PBLH diurnal cycle.

https://doi.org/10.5194/acp-2019-764
Preprint. Discussion started: 30 September 2019

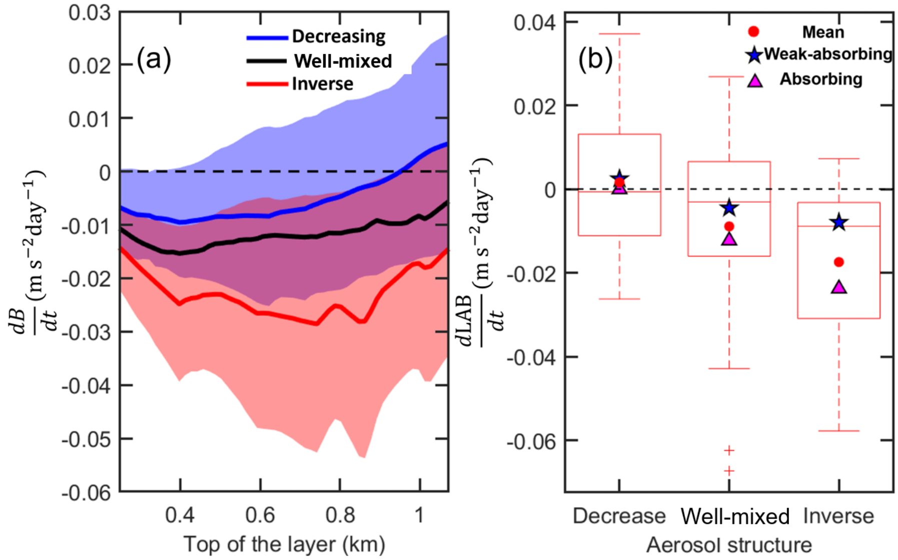

Figure 8. (a) The change rate in buoyancy (dB/dt) in a certain layer of lowest atmosphere under decreasing (blue), well-mixed (black), and inverse (red) aerosol structures during noontime. The change rate at the bottom of the layer is zero, and that in buoyancy is subjected to the top of the layer. The shaded areas show the standard deviation of change rate in buoyancy. (b) Box-and-whisker plots showing 10th, 25th, 50th, 75th, and 90th percentile values of change rate in LAB (buoyancy within lowest 1km) during noontime. The red dots indicate the mean values, while the blue stars and pink triangles show means for weak-absorbing (SSA>0.9) and absorbing (SSA<0.85) cases.

https://doi.org/10.5194/acp-2019-764
Preprint. Discussion started: 30 September 2019

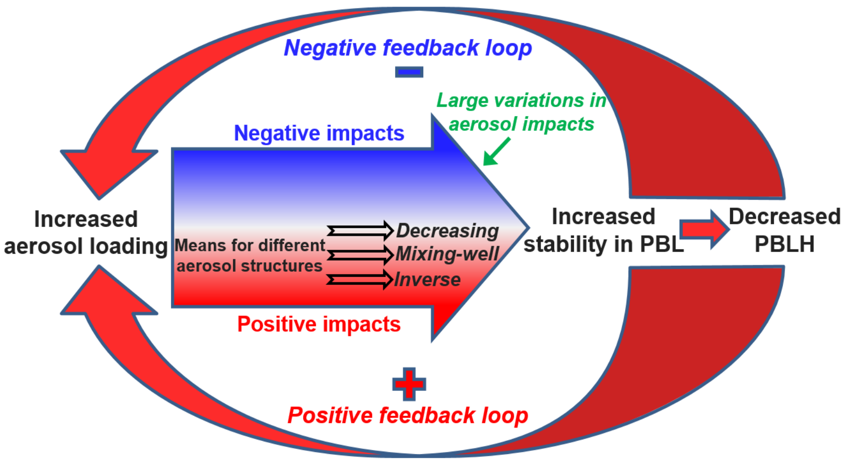

Figure 9. Schematic diagram showing the interactions between aerosols, stability, and the PBL that comprise positive impacts (red arrows) and negative impacts (blue arrows). The aerosol impacts on stability largely vary with meteorology and aerosol conditions, and the means of aerosol impacts on stability for different aerosol structures are indicated in the diagram.